Effects of Annular-finned Tube Deformation on Thermal Stresses in a Heat Exchanger

M. Kashani, A. Hatami*, M. Hosseini

Faculty of Mathematics, University of Sistan and Baluchestan, Zahedan, Iran

ABSTRACT: Nowadays, along with the developments in the industry, many machines and structures are exposed to very high-temperature environments, which has caused various types of thermal load in them. These conditions have led to focused studies on thermal stresses in structures. Heat exchangers are among the structures in which the temperature difference causes thermal stress. In this paper, "finite volume" and "finite element" methods are used to solve flow equations and thermal stress equations in solids, respectively. In addition, the effect of changes in the shape of the annular finned pipe on the thermal stresses in the heat exchanger is investigated. The study results on changing the pipe shape from circular to elliptical show that by changing the pipe shape, the thermal stress in the fin can be significantly reduced; for instance, in the cases reviewed in this paper, the thermal stress has decreased by 9%. Furthermore, the results of thermal stress show that the Maximum Effective Stress point, both before and after changing the shape, is still located at the fin's base. So, according to the results of this study, examining the effect of pipe shape changing on thermal stress is an imperative measure when designing heat exchangers.

KEYWORDS: Fluid-thermal-structural analysis, Annular fin, Thermal stress, Turbulent flow, Heat exchanger

[Received May 19, 2022; Revised Aug. 11, 2022; Accepted Aug. 22, 2022] Print ISSN: 0189-9546 | Online ISSN: 2437-2110

NOMENCLATURE

English symbols

c_p	Specific heat at constant pressure, j/kgk
E	Modulus of elasticity, Pa
H	Convective heat transfer coefficient, W/m^{2}k
k^f	Thermal conductivity, W/mk
k_t	turbulent thermal conductivity, W/mk
R	Radius, m
r_b	Inner radius of the fin, m
r_e	Outer radius of the fin, m
S_{rr}	Radial stress
$S_{\theta\theta}$	Tangential stress
$S_{r\theta}$	Shear tress
T	Temperature, k
T_a	Fluid temperature, k
T_b	Temperature at the fin base, k
u	Displacement, m
w_t	Fin thickness, m

Greek symbols

α	Surface absorptivity
α^*	Thermal expansion coefficient
ε	Surface emissivity
ε_{rr}	Radial strain
$\varepsilon_{\theta\theta}$	Tangential strain
υ	Poisson's ratio
ρ	Density, kg/m^3
μ	Dynamic viscosity, kg / m.s
μ_t	Turbulent viscosity, kg / m.s

I. INTRODUCTION

Engineers strive to improve heat transfer from mechanical devices and researchers from various engineering backgrounds have proposed numerous techniques for this purpose. Using fins is considered a versatile straightforward solution. Thanks to their simple structure and low cost, fins are abundantly used in various applications including aviation, automotive, electronics, and other industries. Fins improve heat transfer by increasing the surface-to-volume ratio. However, the resulting temperature gradient brings about thermal stresses, and thus damages the fin structure. This has prompted researchers to carry out extensive studies on fin temperature distribution and thermal stresses. Some of these works on annular fins are reviewed in what follows.

Using the inverse Laplace transform and Simpson's rule, Shang-Sheng (Wu, 1997) investigated transient thermal stresses in a uniform, isotropic annular fin, assuming one-dimensional heat transfer. Yu and Chen (Yu & Chen, 1999) used a hybrid one-dimensional method to study steady-state and transient stresses and heat transfer in an isotropic annular fin under convection, radiation, and convection–radiation boundary conditions. They compared the resulting temperature distributions and stresses using various boundary conditions. Chio and Chen (Chiu & Chen, 2002) used decomposition to study temperature and thermal stress distribution across an isotropic annular fin. Their results showed that even small temperature perturbations have a significant impact on thermal

*Corresponding author: ahatami@math.usb.ac.ir

doi: http://dx.doi.org/10.4314/njtd.v19i4.2

stresses. Roy and Ghosal (Roy & Ghosal, 2017) used the Homotopy Perturbation Method (HPM) to investigate temperature distribution across an annular fin and the effect of temperature-induced variations of thermal conductivity coefficient on fin's efficiency and temperature distribution. Peng and Chen (Peng & Chen, 2011) also studied temperature distribution across the annular fin using hybrid differential transforms and finite-difference methods. (Roozbahani, *et al*., 2017) used the Homotopy Analysis Method (HAM) to find the temperature and stress distributions across an annular disc.

Other works include that of (Aziz, 1993), who investigated the two-dimensional conductivity of a rectangular fin addressing the effect of thermal source, non-uniform fin base (inner radius) temperature, and changes in convective heat transfer coefficient. (Lau & Tan, 1973) focused on errors in one-dimensional heat transfer analysis of straight annular fins. They proposed a two-dimensional analytical solution for a fin with a constant base temperature and a locally invariant convective heat transfer coefficient around the fin. (Sharma, *et al*., 2019) calculated temperature and thermal stress gradients in an annular fin. They presented their results for different aspect ratios (ratio of inner to outer radii) by changing the annular fin inner radius. They obtained a second-order nonlinear differential equation as the governing equation for all parameters. (Hatami & Ganji, 2013) used the fourth-order Runge–Kutta method to examine heat transfer from the surface of annular fins with rectangular, triangular, convex, and power-law cross sections.

They considered aluminum, copper, and silicon nitride fins and showed that the fin made of silicon nitride with a power-law cross-section maximized heat transfer. (Nagarani, *et al.*, 2014) reviewed previous studies on bringing extended surfaces into heat transfer problems in heat exchangers. Their results help select extended surfaces with different geometries based on available space and costs. In an experimental–numerical study, (Jang, *et al*., 1998) investigated the performance of an annular tube bundle comprising four rows of annular-finned tubes in dry and wet conditions for inlet velocities in the range of 1–6 m/s. They showed that using a one-dimensional model with increasing flow velocity causes an increase in fin efficiency estimation errors. (Mon & Gross, 2004) adopted a numerical method to study the effects of fin spacing on heat transfer, pressure drop, and flow behavior in a four-row annular-finned tube bundle under turbulent conditions. They showed that boundary layer development around the fin and tube surface primarily depends on the ratio of fin spacing to fin height.

Further, their results showed that, increasing this ratio in a linear arrangement increases the heat transfer coefficient while reducing pressure drop. Drawing on (Mon & Gross, 2004) works, (Bilirgen, *et al*., 2013) addressed the case of one row of annular-finned tubes under turbulent flow conditions and carried out on a detailed investigation of the effect of Reynolds number (Re), fin spacing, fin height, fin thickness, and fin material, on heat transfer and pressure drop. They showed that fin thickness has a much less significant effect on heat transfer and pressure drop than fin height and spacing. (Jang & Yang, 1998) studied numerically and experimentally pressure drop and heat transfer in elliptical and annular-finned tube bundles with inlet velocities in the range of 2–7 m/s. They showed that the heat transfer coefficient of an annular-finned tube is 20–50% higher than that of an elliptical-finned tube with identical tube (geometry). However, circular tubes were found to experience a higher pressure drop than elliptical ones.

(Hu & Jacobi, 1993) carried out numerical and experimental investigations of heat transfer in a four-row annular tube bundle. It was shown that in the Re = 3300–12000 range, a considerable change is observed in convective mass transfer and mass transfer behavior even for an infinitesimal angle of attack. (Mon, 2003) studied the effects of geometrical parameters, including fin thickness, fin height, tube diameter, fin pitch, and the annular-finned tube bundle arrangement on the heat transfer coefficient. It was shown that increasing the fin-spacing-to-fin-height ratio increases the heat transfer coefficient and reduces pressure drop in a linear arrangement. However, doing the same in a staggered arrangement initially increases the heat transfer coefficient before reducing it. (Shokouhmand, *et al*., 2014) optimized an annular-finned tube through structural design aiming to find the optimal geometry that maximized heat exchange. It was shown that the optimal geometry depends on flow conditions. In a numerical study, (Nemati & Moghimi, 2014) investigated flow in finned tube bundles of heat exchangers with various types of turbulence. Their results indicated that the Transition SST model is consistent with experimental results. Moreover, (Nemati & Samivand, 2016) used Transition SST and investigated flow and heat transfer in annular and elliptical-finned tubes.

(Kundu & Das, 2007) used a semi-analytical method to study elliptical fins. Their study showed that an optimal elliptical fin could dissipate heat at a much higher rate than a circular fin. The study recommended considering the fin volume or heat dissipation rate as the constant parameter in optimizing the fin geometry. (Jang & Yang, 1998) also published a research on elliptical fins. Their experimental–numerical study addressed flow and heat transfer in a four-row assembly of elliptical-finned tubes with alternating and linear arrangements. They also studied a circular-finned tube with an alternating arrangement. Their experimental results showed that the heat transfer coefficients of elliptical-finned tubes were 35–50% of that of circular-finned tubes of the same perimeter, whereas the total pressure drop in the assembly was only 25–30% of that in the circular-finned tubes. Furthermore, (Nagarani, *et al*., 2014) also discussed the advantages of elliptical fins and tubes compared to other geometries. These advantages can be listed as follows:

- By using elliptical fins, the pressure drop across circular tubes can be reduced.
- Space limitation in one side and sufficient space in the vertical direction improves the heat transfer rate.
- Oblong tubes with a principal axis parallel to the flow direction generally enhance heat transfer.
- Furthermore, this design allows extension of the external surface, improving overall heat transfer. This prompted several studies on heat transfer and hydrodynamics of non-circular tubes and tube (Hatami, *et al*., 2020) assemblies.
- A non-circular geometry reduces scaling due to the small surface area of the front portion of the tubes and their smaller separation zone.

- There is increasing power density with in a given volume and envelope shape

A review of previous studies on annular fins showed that the extensive applications of fins across different industries had inspired several experimental, numerical, or analytical studies. Some researchers have focused on the effect of temperature on annular fins thermal stresses and strains (Wu, 1997; Chiu & Chen, 2002; Bidzard, *et al*., 2017; Hatami, *et al*., 2020). The present study relied on the fluid-thermal-structural analysis to investigate the deformations of the annular-finned tube and its effects on thermal stresses in heat exchangers. This study draws on research by (Hosseini, *et al*., 2020; Hosseini, *et al*., 2020), who investigated the effects of the deformation of tubes in the first row of fin bundles. The aim was to investigate the effects of tube deformation in other rows of fin bundles.

II. PROBLEM DESCRIPTION AND GOVERNING EQUATIONS

A. *Problem Description*

Figures 1 and 2 illustrate the problem geometry. The turbulent flow of air runs at 0.002 kg/s around the fin with an initial surface temperature of T_{sur} = 300 K. At T_b = 600 K, the tube wall temperature was also assumed to be constant and equal to the base (inner radius) temperature. Tables 1 and 2 present geometrical conditions and fin material, respectively. This study investigated thermal stresses deforming the tube into an elliptical shape as depicted in Figure 2. Since the sharpest temperature gradient in the heat exchanger develops during the initial moments, all discussions in this study are limited to the instant after 10 seconds.

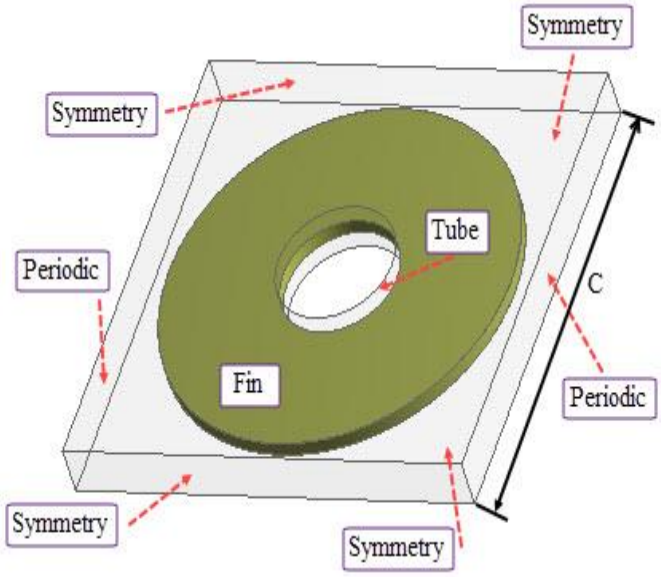

Figure 1: Three-dimensional annular fin geometry.

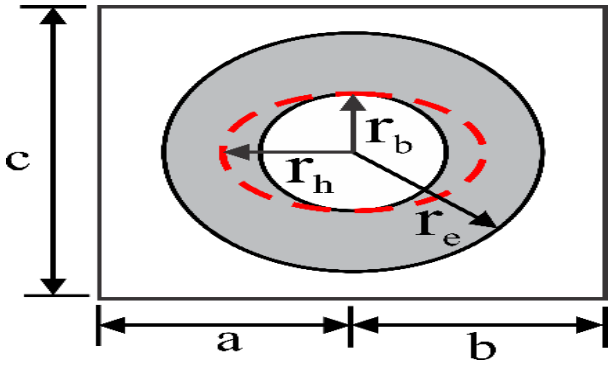

Figure 2: Tube deformation.

Table 1: Geometrical specifications.

Distance from inlet	a = 10 mm
Distance from outlet	b = 10 mm
Solution domain height	h = 14 mm
Solution domain width	c = 140 mm
Fin thickness	w_t = 4 mm
Base radius	r_b = 20 mm
Tip radius	r_e = 60 mm

Table 2: Fin material properties.

Density	$\rho^s = 2700\ kg/m^3$
Young's modulus	$E^s = 71000\ MPa$
Poisson's ration	$\nu^s = 0.33$
Specific heat	$c^s_p = 925\ J/KgK$
Coefficient of thermal expansion	$\alpha^{*s} = 2.3\times10^{-5}\ C^{-1}$
Tensile yield strength	280 MPa
Tensile ultimate strength	310 MPa
Compressive yield strength	280 MPa

B. *Governing Equations and Boundary Conditions*

1) *Fluid domain*

Equations governing heat transfer and flow under transient, turbulent, three-dimensional, and incompressible conditions are (Nemati & Samivand, 2016).

A- Continuity equation:

$$\frac{\partial \rho}{\partial t} + \frac{\partial}{\partial x_i}(\rho u_i) = 0 \qquad (1)$$

B- Momentum equation:

In Eqn. (2), μ is the dynamic viscosity, μ_r is the turbulent viscosity, and k is the turbulent kinetic energy.

$$\frac{\partial u_i}{\partial t} + \rho\frac{\partial}{\partial x_j}(u_i u_j) = -\frac{\partial p}{\partial x_j} + \frac{\partial}{\partial x_j}\left[\mu\left(\frac{\partial u_i}{\partial x_j} + \frac{\partial u_j}{\partial x_i} - \frac{2}{3}\delta_{ij}\frac{\partial u_i}{\partial x_i}\right)\right] + \frac{\partial}{\partial x_j}\left(-\overline{u_i' u_j'}\right)$$

$$-\overline{u_i' u_j'} = \mu_t\left(\frac{\partial u_i}{\partial x_j} + \frac{\partial u_j}{\partial x_i}\right) - \frac{2}{3}\left(\rho k + \mu_t\frac{\partial u_l}{\partial x_l}\right)\delta_{ij} \qquad (2)$$

C- Energy equation:

$$\frac{\partial(\rho E+p)}{\partial t}+\frac{\partial}{\partial x_i}(u_i(\rho E+p))=\frac{\partial}{\partial x_i}\left[(k+k_t)\frac{\partial T}{\partial x_i}\right] \quad (3)$$

In Eqn. (3), *E* is the total energy.

D-Boundary conditions:

i. Inlet and outlet boundary conditions:

Periodic boundary conditions for the inlet and outlet (Patankar, *et al*., 1977) are as follows:

$$u_{inlet}=u_{outlet},\ v_{inlet}=v_{outlet},\ w_{inlet}=w_{outlet}$$

$$\dot{m}_{inlet}=\dot{m}_{outlet}$$

$$\Theta_{inlet}=\Theta_{outlet},\ \Theta=\frac{T-T_b}{T_{bulk}-T_b},\ T_{bulk}=\frac{\int_0^A \rho u c_p T\,dA}{\int_0^A \rho u c_p\,dA} \quad (4)$$

ii. The symmetry boundary condition for the surfaces shown in Figs. 1 and 2 are as follows:

$$\frac{\partial u_i^f}{\partial x_2}=0,\ \frac{\partial u_i^f}{\partial x_3}=0$$
$$\frac{\partial T^f}{\partial x_2}=0,\ \frac{\partial T^f}{\partial x_3}=0 \quad (5)$$

iii. The no-slip condition defined for the tube and the fin is:

$$u_i^f=0 \quad (6)$$

In Eqns. (5) and (6), u_i^f is the component i of the fluid velocity.

2) Solid domain (fin)

The equations governing the solid domain include energy, equilibrium, constitutive, and strain–displacement equations. An important assumption here is to consider the energy equation to be independent of the equilibrium, constitutive, and strain–displacement equations. In other words, the energy equation is solved first using the thermal boundary conditions. The resulting temperature is used subsequently in solving the other three equations.

Moreover, the fins physical properties were assumed to be uniform and isotropic. Given the small fin thickness, the equations governing the solid domain were solved using the plane-stress assumption. A constant temperature thermal boundary condition was used at the fin base and a coupled boundary condition between the fin and the fluid to solve the energy equation. The zero-radial-stress boundary condition was used to solve the equilibrium, constitutive, and strain–displacement equations for the fin base and the outer radius. Moreover, the axial stress was assumed to be zero normal to the fin (in the *z* direction). The solid domain equations are presented as follows.

i. Energy equation and its boundary conditions:

$$\sigma_{rr}=\frac{E}{1-\nu^2}[\varepsilon_{rr}+\nu\varepsilon_{\theta\theta}-(1+\nu)\alpha^*\Delta T]$$
$$\sigma_{\theta\theta}=\frac{E}{1-\nu^2}[\varepsilon_{\theta\theta}+\nu\varepsilon_{rr}-(1+\nu)\alpha^*\Delta T] \quad (7)$$
$$\tau_{r\theta}=\frac{E}{1+\nu}\varepsilon_{r\theta}$$

In Eqn. (7), T^s is the temperature, ρ^s is the density, k^s is the thermal conductivity, and c_p^s is the special heat capacity of the fin.

i. Equilibrium equations:

In the absence of body forces, the two equilibrium equations are as follows:

$$\frac{\partial\sigma_{rr}}{\partial r}+\frac{1}{r}\frac{\partial\tau_{r\theta}}{\partial\theta}+\frac{(\sigma_{rr}-\sigma_{\theta\theta})}{r}=0$$
$$\frac{\partial\tau_{r\theta}}{\partial r}+\frac{1}{r}\frac{\partial\sigma_{\theta\theta}}{\partial\theta}+\frac{2\tau_{r\theta}}{r}=0 \quad (8)$$

where σ_{rr} and $\sigma_{\theta\theta}$ are the radial and tangential stresses, respectively.

ii. Constitutive equations:

$$\sigma_{rr}=\frac{E}{1-\nu^2}[\varepsilon_{rr}+\nu\varepsilon_{\theta\theta}-(1+\nu)\alpha^*\Delta T]$$
$$\sigma_{\theta\theta}=\frac{E}{1-\nu^2}[\varepsilon_{\theta\theta}+\nu\varepsilon_{rr}-(1+\nu)\alpha^*\Delta T] \quad (9)$$
$$\tau_{r\theta}=\frac{E}{1+\nu}\varepsilon_{r\theta}$$

where E denotes the elastic modulus, υ is Poisson's ratio, and α^* is the thermal expansion coefficient.

iii. Strain–displacement equations:

$$\varepsilon_{rr}=\frac{\partial u_r}{\partial r},\ \varepsilon_{\theta\theta}=\frac{u_r}{r}+\frac{1}{r}\frac{\partial u_\theta}{\partial\theta},\ \varepsilon_{r\theta}=\frac{1}{2}\left(\frac{1}{r}\frac{\partial u_r}{\partial\theta}+\frac{\partial u_\theta}{\partial r}-\frac{u_\theta}{r}\right) \quad (10)$$

iv. Boundary conditions for the equilibrium, constitutive, and strain–displacement equations:

$$(\sigma_{rr})_{r_b}=0,\ (\sigma_{rr})_{r_c}=0$$
$$u_r=\text{Free},\ u_\theta=0,\ u_z=0 \quad \text{at} \quad r=r_b$$
$$u_r=\text{Free},\ u_\theta=0,\ u_z=\text{Free} \quad \text{at} \quad r=r_c \quad (11)$$
$$u_r=\text{Free},\ u_\theta=0,\ u_z=\text{Free} \quad \text{at} \quad z=-2\text{mm}$$
$$u_r=\text{Free},\ u_\theta=0,\ u_z=\text{Free} \quad \text{at} \quad z=2\text{mm}$$

where u_r, u_θ, and u_z are displacements along *r*, *θ*, and *z*, respectively.

S_{rr} and $S_{\theta\theta}$ are defined as given in Eq. (12) and (13) respectively.

$$S_{rr} = \frac{\sigma_{rr}}{\alpha^* E} \tag{12}$$

$$S_{\theta\theta} = \frac{\sigma_{\theta\theta}}{\alpha^* E} \tag{13}$$

ii. Solid-Fluid Interface Domain

The following boundary condition holds over the fin–fluid interface.

$$k^s \frac{\partial T^s}{\partial n} = k^f \frac{\partial T^f}{\partial n}, \quad T^s = T^f \tag{14}$$

where n is the direction normal to the surface.

III. GRID AND VALIDATION

A. *Grid*

The grid types used in the solution domain for the fins and the fluid are illustrated in Figures 3 and 4, respectively.

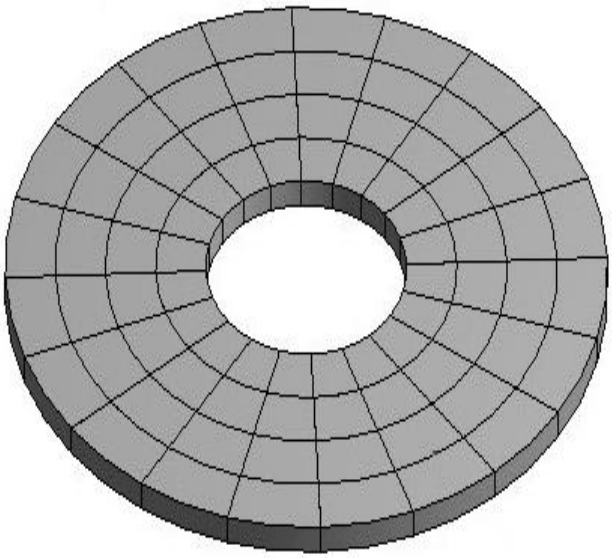

Figure 3: Structured mesh for the fin.

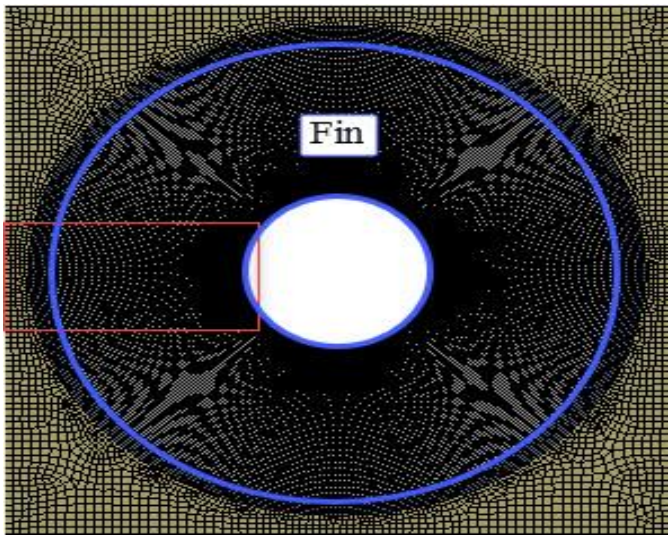

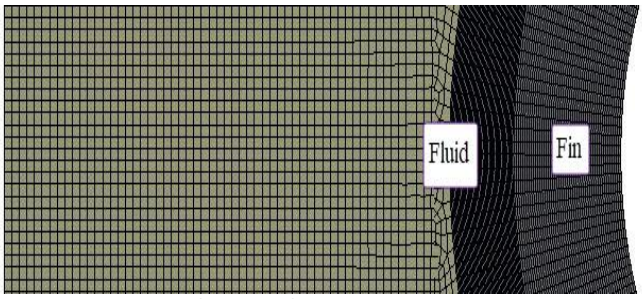

Figure 4: The magnified mesh for the rectangular region.

B. *Validation*

1) *Solid domain*

In order to validate the solid-domain results, the radial and tangential stresses and the annular fin temperature were compared against similar reports from the literature (Chiu & Chen, 2002; Roy & Ghosal, 2017; Peng & Chen, 2011). As evident from Fig. 5, the radial stress results are consistent with the results of (Chiu & Chen, 2002) with a 0.3% relative error. Also, reasonable accuracy was observed in the tangential stress as shown in Fig. 6. The temperature distribution results are also compared in Tables 3, 4, 5, 6 and 7 with corresponding results from the literature (Chiu & Chen, 2002; Roy & Ghosal, 2017; Peng & Chen, 2011). According to (Chiu & Chen, 2002; Roy & Ghosal, 2017; Peng & Chen, 2011), $\xi = r - r_b / r_e - r_b$ and $\xi^* = r/r_b$.

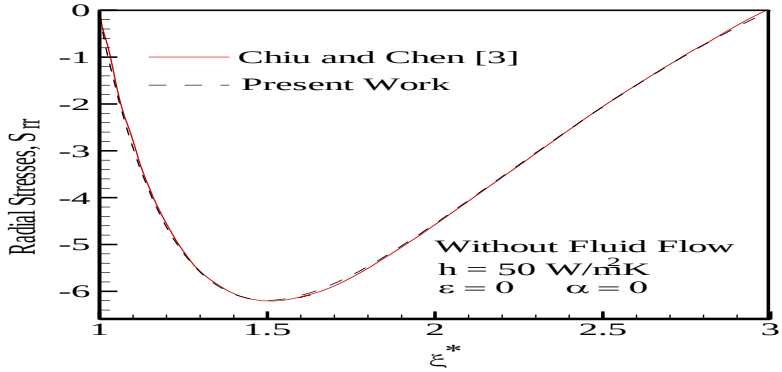

Figure 5: Comparison of radial stresses.

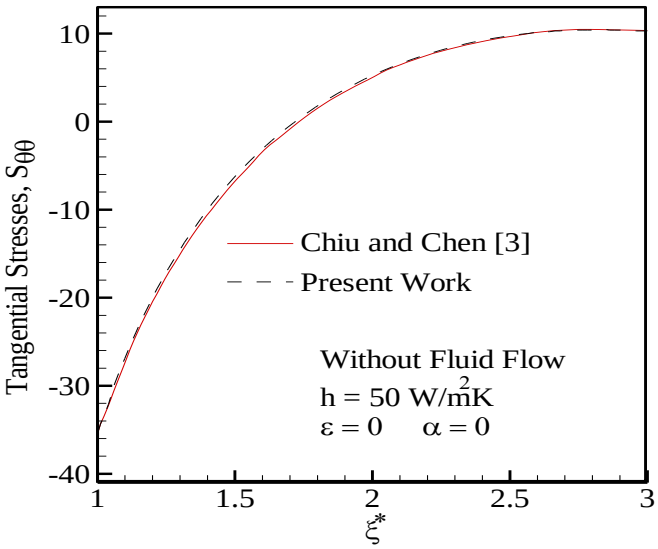

Figure 6. Comparison of Tangential stresses.

Table 3: Comparison of temperature values (Kelvin) at specific locations (insulated boundary condition for the fin tip and convection boundary condition for the fin's top and bottom surfaces).

Solution method	$\xi = 0.$	$\xi = 0.50$	$\xi = 0.75$	$\xi = 1.00$
Roy & Ghosal, 2017)	578.52	566.28	560.19	558.3
Present work	578.45	566.35	560.19	558.36

Table 4: Comparison of temperature values (Kelvin) at specific locations (convection boundary condition for the fin tip and its top and bottom surfaces).

Solution method	$\xi = 0.25$	$\xi = 0.50$	$\xi = 0.75$	$\xi = 1.00$
(Chiu & Chen, 2002)	557.070	563.724	556.613	554.022
(Roy & Ghosal, 2017)	557.826	565.053	558.482	556.513
(Peng & Chen, 2011)	576.99	563.88	556.86	554.31
Present work	576.98	563.90	556.86	554.33

2) Fluid domain

For the fluid domain, validation was performed by comparing the results of the present numerical solution with the experimental (Verein Deutscher Ingenieure, 2000) and numerical (Mon, 2003) results. All conditions are similar to the i1 case in page 152 from Mon,s thesis (Mon, 2003).

$$Nu = 0.22\,Re^{0.6}\,Pr^{\frac{1}{3}}\left(\frac{A}{A_t}\right)^{-0.15},\ \text{Maximum deviation} \pm 25\%, \quad (15)$$

IV. RESULTS AND DISCUSSION

This section discusses the effect of changes in r_h on the temperature and effective stress. Figure 7 shows the directions of the angles.

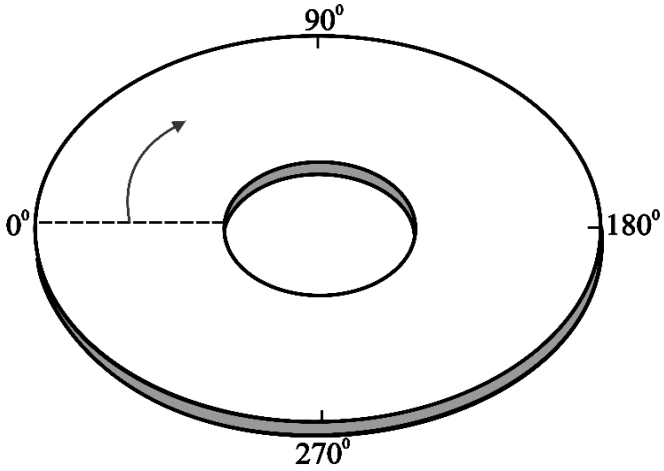

Figure 6: Comparison of tangential stresses.

A. Temperature Variations

Figure 8 shows temperature contours in the fin for circular and elliptical tubes with respect to r_h. These contours show that increasing r_h reduced temperature gradient in the radial direction. The reduction was even more substantial at *0°*, which corresponds to the maximum effective stress (Hosseini, *et al*., 2020). It is also observed that the temperature gradient intensified in the θ direction as tube deformed.

Table 5: Comparison of radial stresses values at specific locations (insulated boundary condition for the fin tip and convection boundary condition for the fin's top and bottom surfaces).

Solution method	$\xi^* = 1$	$\xi^* = 1.50$	$\xi^* = 2.00$	$\xi^* = 2.50$	$\xi^* = 3.00$
(Chiu & Chen, 2002)	0	-6.20	-4.60	-1.95	0
Present work	0	-6.21	-4.60	-1.95	0

Table 6: Comparison of Tangential stresses values at specific locations (insulated boundary condition for the fin tip and convection boundary condition for the fin's top and bottom surfaces).

Solution method	$\xi^* = 1$	$\xi^* = 1.50$	$\xi^* = 2.00$	$\xi^* = 2.50$	$\xi^* = 3.00$
(Chiu & Chen, 2002)	-34.62	-6.49	4.90	9.79	10.41
Present work	-34.62	-6.50	4.90	9.79	10.41

Table 7: Fluid-domain validation results.

Nu (Verein Deutscher Ingenieure, 2000)	Nu (Mon, 2003)	$Nu_{present\ work}$	$Err_{with\ Experimental}$	$Err_{with\ Numerical}$
34.00	34.40	32.21	5.26%	6.37%

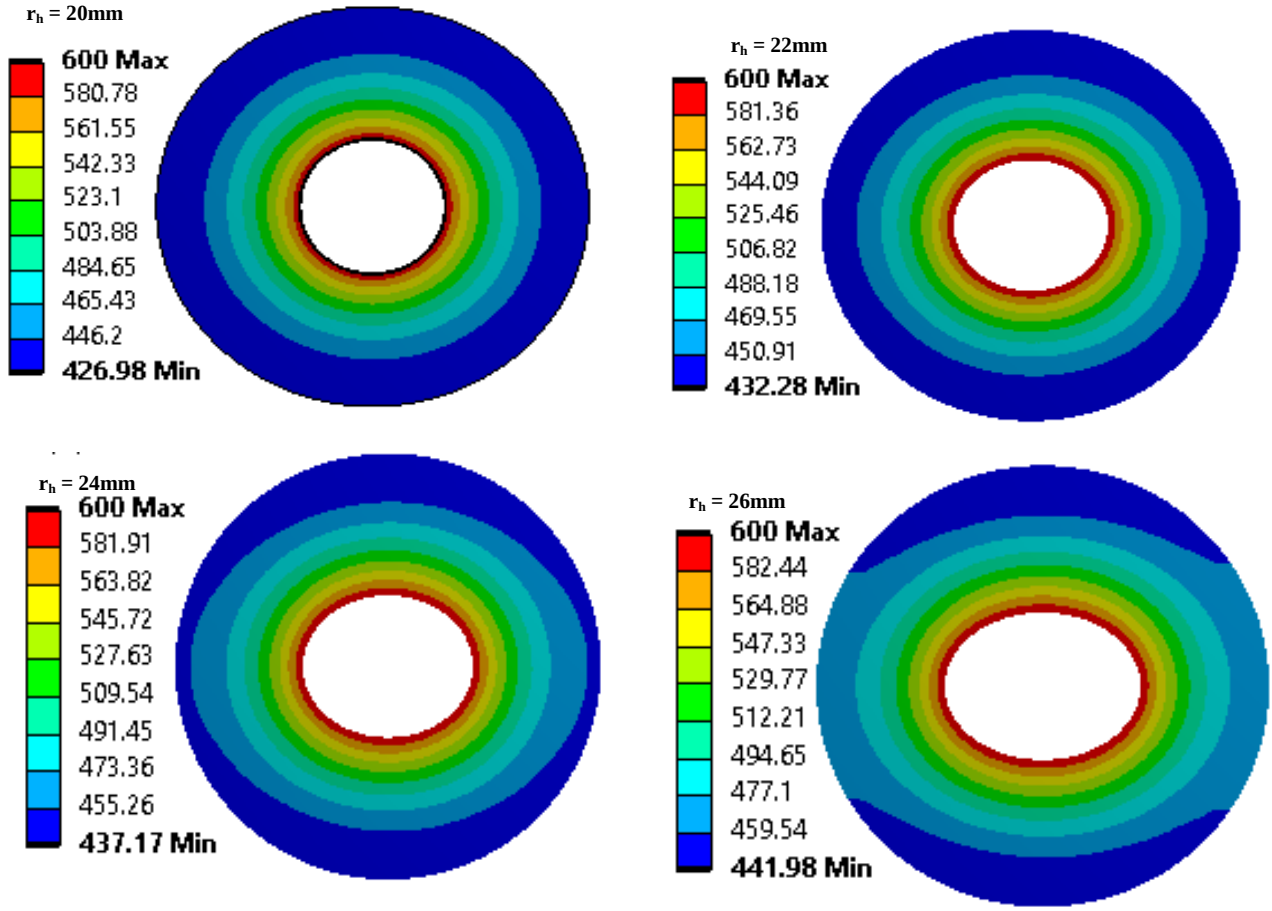

Figure 8: Temperature contours of the fin.

B. Radial, Tangential and Shear Stress Variations

Figures 9–11 depict radial, tangential, and shear stress contours. These contours show that radial and tangential stresses decreased as the initially circular tube deformed into an elliptical shape and the shear stress increased due to the temperature gradient being intensified along θ.

It is observed that the peak radial stress occurred in the same areas with the steepest radial temperature gradient. Figure 10 indicate that the largest absolute values of the tangential stress before and after deformation occurred at the fin base, where it is attached to the tube. Furthermore, the results show that the tangential stresses are predominantly affected by temperature.

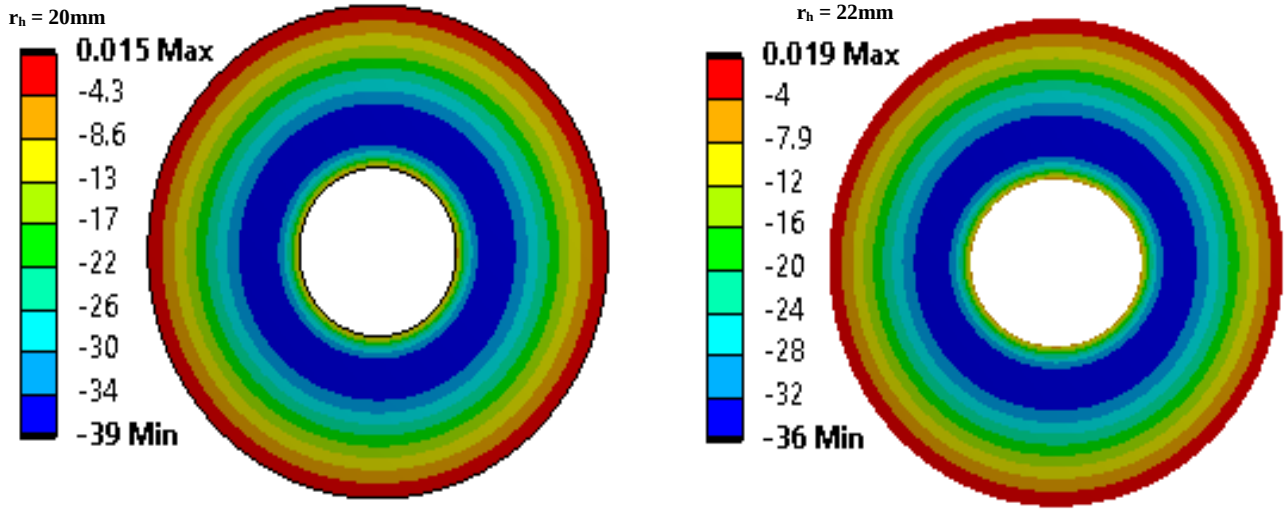

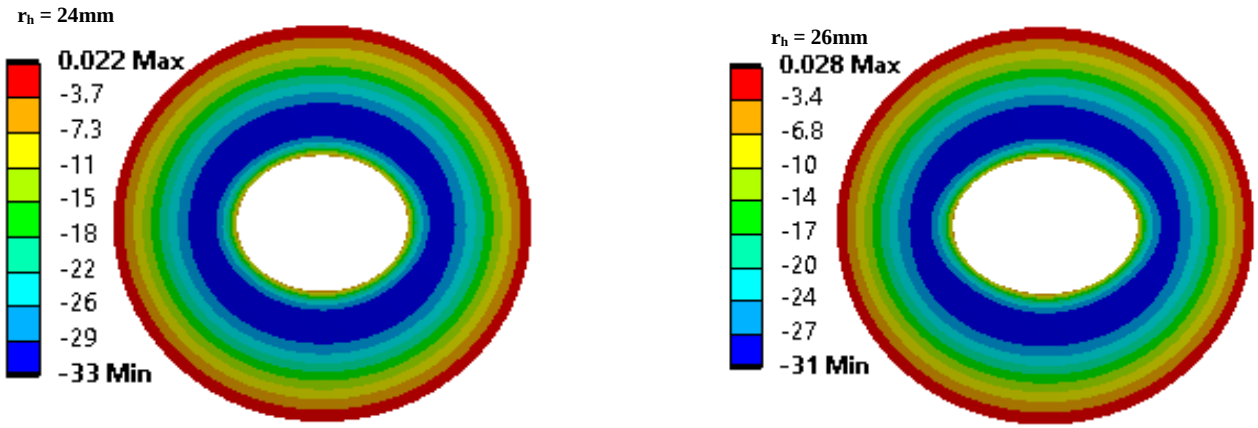

Figure 9: Radial stress contours.

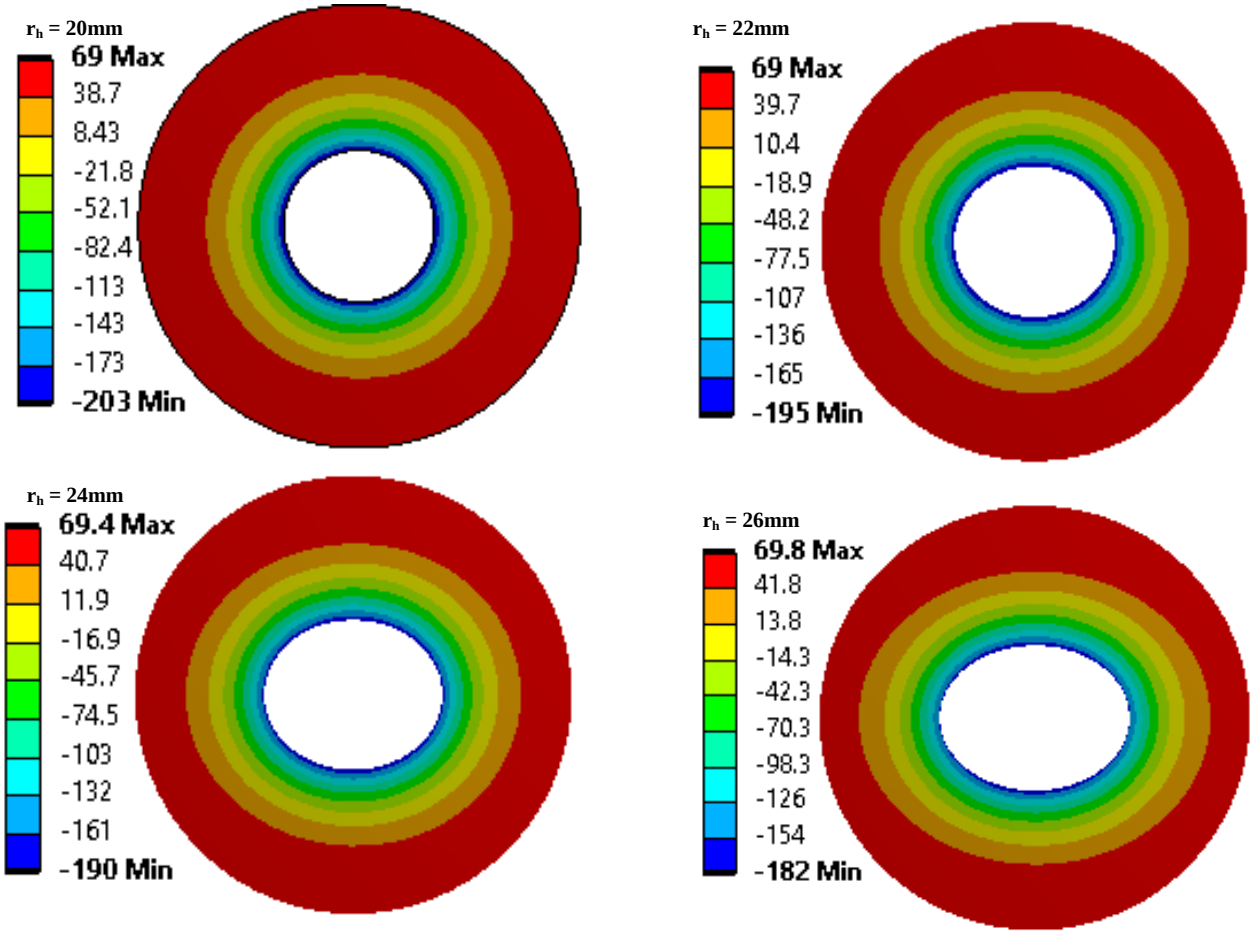

Figure 10: Tangential stress contours.

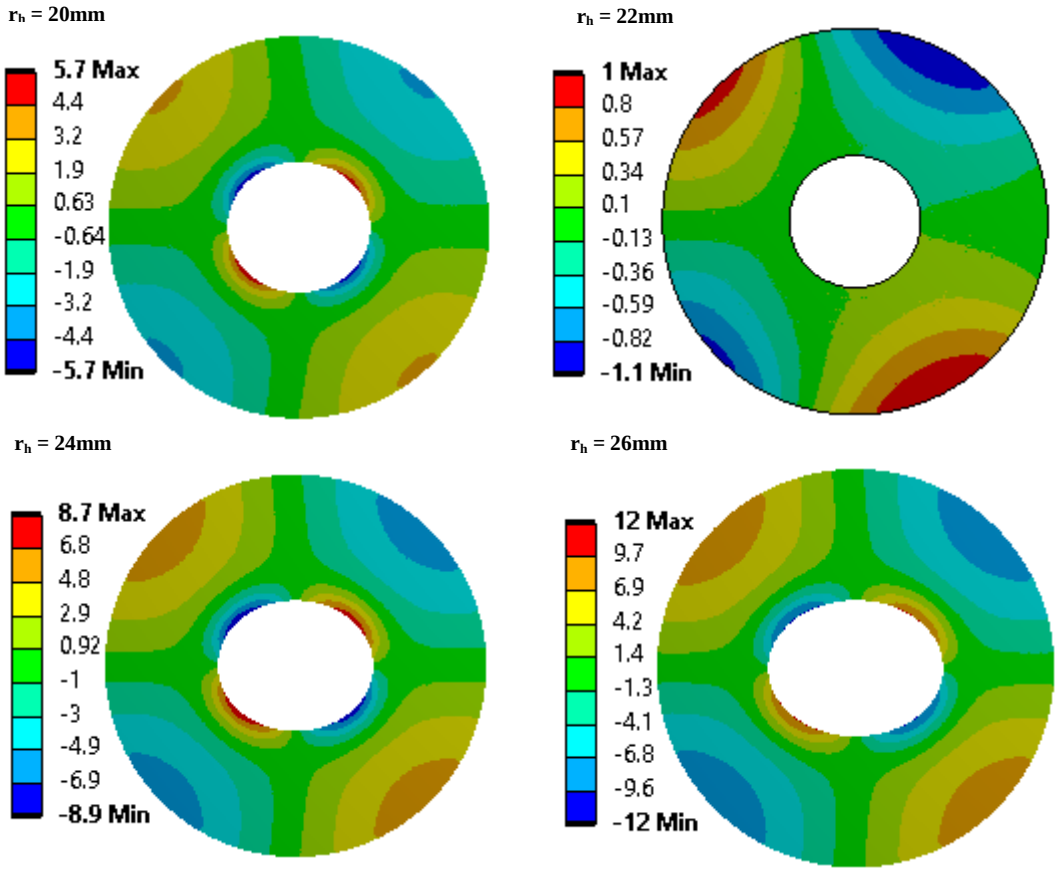

Figure 11: Shear stress contours.

C. Effective Strain and Strain Variations

The effective thermal stress serves as the criterion for determining the critical points in terms of strength and deformation. Figure 12 depicts effective stress contours. The effective stress equation used in this study is presented in Eqn. 16.

Figure 12 shows that the tube deformation from a circular to an elliptical shape reduced the effective stress by 9%. The maximum effective stress occurred at the fin base. It was also found that the tube deformation changed the distribution of effective stress in the fin along θ due to an increase in the shear stress.

$$\sigma_{ef} = \sqrt{2\sigma_{rr}^2 + 2\sigma_{\theta\theta}^2 - 2\sigma_{rr}\sigma_{\theta\theta} + 6\sigma_{r\theta}^2} \qquad (16)$$

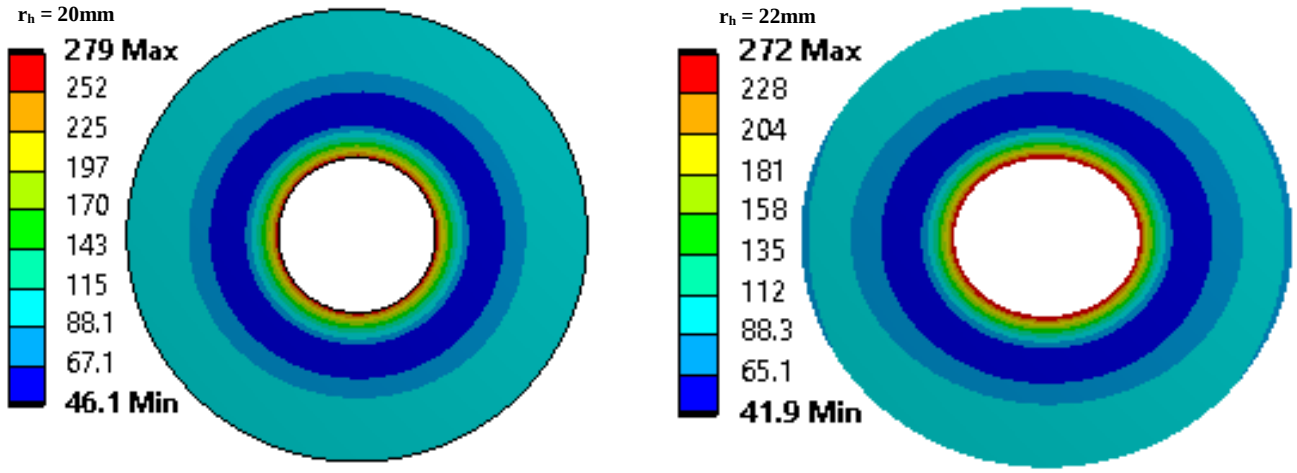

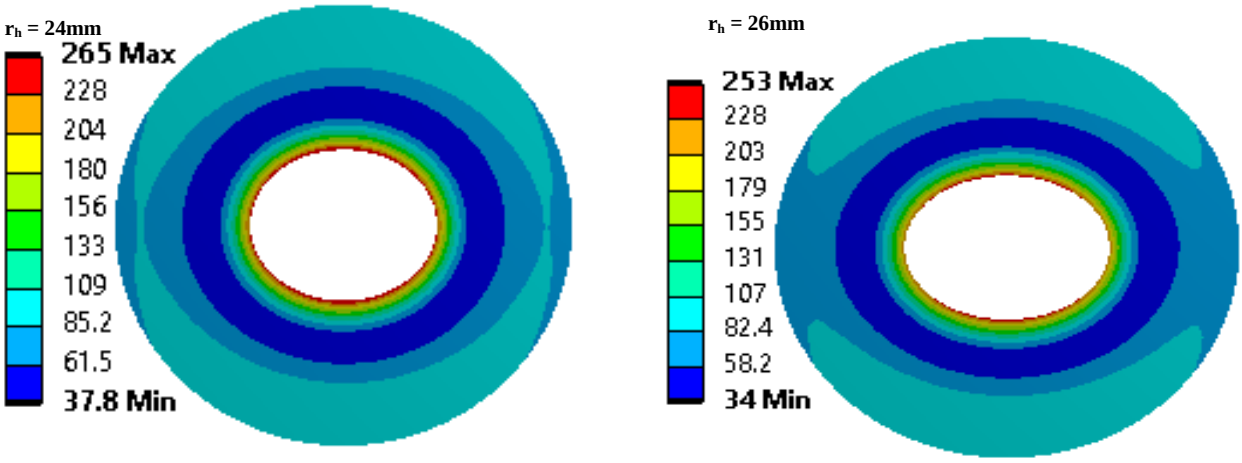

Figure 12: Effective stress contours.

V. CONCLUSION

The effects of deformation of an annular finned tube from a circular to an elliptical shape on its thermal stresses were investigated and critical points of the fin in terms of thermal stress were determined. The finite-volume method and Transition SST model were coupled with the SIMPLE algorithm to solve flow equations, while the thermal stress equations were solved in the solid domain by the finite-element method. The results can be summarized as follows:

- Overall, it is concluded that using elliptical-finned tubes significantly reduces the effective stress.
- The maximum effective stress before and after deformation consistently remained at the base of the fin.
- Tube deformations reduced radial and tangential stresses while increasing shear stress.
- The deformation caused the temperature gradient to decrease along *r* but intensified it along θ.

AUTHOR CONTRIBUTIONS

Study concept and design: M**. Kashani**, and **A. Hatami**; analysis and interpretation of data: **M. Kashani**, and **M. Hosseini;** drafting of the manuscript: **M. Kashani;** critical revision of the manuscript for important intellectual content: M**. Kashani**, **A. Hatami**, and **M. Hosseini**; statistical analysis: **M. Kashani**.

REFERENCES

Aziz, A., (1993). The effects of internal heat generation, anisotropy, and base temperature nonuniformity on heat transfer from a two-dimensional rectangular fin. Heat Transfer Engineering, 14(2), 63-70.

Bidzard, A.; M. Mahzoon and M. Yaghoubi. (2017). Analytical Solution for Temperature, Stress and Displacement Fields for a Hollow Cylinder Subjected to Asymmetric and Time Dependent Heat Flux. Amirkabir J. Mech. Eng., Volume 49, 253-260.

Bilirgen, H.; S. Dunbar and E. K. Levy. (2013). Numerical modeling of finned heat exchangers. Applied Thermal Engineering, 61(2), 278-288.

Chiu, C. H. and Chen, C. K. 2002. Application of the decomposition method to thermal stresses in isotropic circular fins with temperature-dependent thermal conductivity. Acta Mechanica, 157, 147-158.

Hatami, A.; P. Samira and M. Hosseini. (2020). Numerical analysis of thermal stresses and strains of annular finned tube bundle in turbulent flow regime. *Mechanics & Industry*, 21(6), 601.

Hatami, M. and Ganji, D. D. (2013). Thermal performance of circular convective–radiative porous fins with different section shapes and materials. Energy Conversion and Management, Volume 76, 185-193.

Hosseini, M.; A. Hatami and S. Payan. (2020). Comparison of the effect of laminar and turbulent flow regimes on thermal stresses and strains in an annular fin. Journal of Mechanical Science and Technology, 34(1), 413-424.

Hosseini, M.; A. Hatami and S. Payan. (2020). Impact of Flow around Annular Fins on their Thermal Stresses and Strains. Amirkabir J. Mech. Eng., 52(1), 51-54.

Hu, X. and Jacobi, A. M. (1993). Local Heat Transfer Behavior and Its Impact on a Single-Row, Annularly Finned Tube Heat Exchanger. ASME. J. Heat Transfer, 115(1), 66-74.

Jang, J. Y. and Yang, J.-. Y. (1998). Experimental and 3-D numerical analysis of the thermal-hydraulic characteristics of elliptic finned-tube heat exchangers. Heat Transfer Engineering, 19(4), 55-67.

Jang, J. Y.; J. T. Lai and L. C. Liu. (1998). The thermal-hydraulic characteristics of staggered circular finned-tube heat exchangers under dry and dehumidifying conditions. International journal of heat and mass transfer, 41(21), 3321-3337.

Kundu, B. and Das, P. K. (2007). Performance analysis and optimization of elliptic fins circumscribing a circular tube. International journal of heat and mass transfer, 50(1-2), 173-180.

Lau, W. and Tan, C. W. (1973). Errors in One-Dimensional Heat Transfer Analysis in Straight and Annular Fins. ASME. J. Heat Transfer, 95(4), 549–551.

Mon, M. S. (2003). Numerical investigation of air-side heat transfer and pressure drop in circular finned-tube heat exchangers, s.l.: Freiberg.

Mon, M. S. and Gross, U. (2004). Numerical study of fin-spacing effects in annular-finned tube heat exchangers.

International journal of heat and mass transfer, 47(8-9), 1953-1964.

Nagarani, N.; K. Mayilsamy; A. Murugesan and G. S. Kumar. (2014). Review of utilization of extended surfaces in heat transfer problems. Renewable and Sustainable Energy Reviews, 29, 604-613.

Nemati, H. and Moghimi, M. (2014). Numerical study of flow over annular-finned tube heat exchangers by different turbulent models. CFD Letters, 6(3), 101-112.

Nemati, H. and Samivand, S. (2016). Numerical study of flow over annular elliptical finned tube heat exchangers. Arabian Journal for Science and Engineering, 41(11), 4625-4634.

Patankar, S. V.; H. Cheng; H. L. Liu and M. S. Ephraim. (1977). Fully developed flow and heat transfer in ducts having streamwise-periodic variations of cross-sectional area. J. Heat Transfer, 99(2), 180-186.

Peng, H. -S. and Chen, C. -L. (2011). Hybrid differential transformation and finite difference method to annular fin with temperature-dependent thermal conductivity. International Journal of Heat and Mass Transfer, 54((11-12)), 2427-2433.

Roozbahani, M. M.; H. Razzaghi; M. Baghani; M. Baniassadi and M. Layeghi. (2017). Temperature and stress distribution in hollow annular disk of uniform thickness with quadratic temperature-dependent thermal conductivity. Journal of Thermal Stresses, 40(17), 828-845.

Roy, R. and Ghosal, S. (2017). Homotopy Perturbation Method for the Analysis of Heat Transfer in an Annular Fin with Temperature-Dependent Thermal Conductivity. ASME. J. Heat Transfer, 139(2), 022001.

Sharma, R.; L. Sondhi; V. K. Gaba and S. Bhowmick. (2019). A Study of Thermo-structural Behavior of Annular Fin. In: Innovative Design, Analysis and Development Practices in Aerospace and Automotive Engineering. Singapore: Springer, 381-387.

Shokouhmand, H.; S. Mahjoub and M. R. Salimpour. (2014). Constructal design of finned tubes used in air-cooled heat exchangers. Journal of Mechanical Science and Technology, 28(6), 2385-2391.

Verein Deutscher Ingenieure. (2000). VDI-Wärmeübergang, Berechnungsblätter fürden Wärmeübergang. 8 ed. Berlin: Springer.

Wu, S. -S., (1997). Analysis on transient thermal stresses in an annular fin. Journal of thermal stresses, 20(6), 591-615.

Yu, L. & Chen, C., (1999). Application of the Hybrid Method to the Transient Thermal Stresses Response in Isotropic Annular Fins. ASME. J. Appl. Mech., 66(2), 340–346.